

Subglacial lava propagation, ice melting and heat transfer during emplacement of an intermediate lava flow in the 2010 Eyjafjallajökull eruption

Björn Oddsson^{1,2} · Magnús T. Gudmundsson¹ · Benjamin R. Edwards³ · Thorvaldur Thordarson⁴ · Eyjólfur Magnússon¹ · Gunnar Sigurðsson⁵

Received: 30 December 2015 / Accepted: 27 May 2016 / Published online: 8 June 2016
© Springer-Verlag Berlin Heidelberg 2016

Abstract During the 2010 Eyjafjallajökull eruption in South Iceland, a 3.2-km-long benmoreite lava flow was emplaced subglacially during a 17-day effusive-explosive phase from April 18 to May 4. The lava flowed to the north out of the ice-filled summit caldera down the outlet glacier Gígjökull. The flow has a vertical drop of about 700 m, an area of ca. 0.55 km², the total lava volume is ca. 2.5·10⁷ m³ and it is estimated to have melted 10–13·10⁷ m³ of ice. During the first 8 days, the lava advanced slowly (<100 m day⁻¹), building up to a thickness of 80–100 m under ice that was initially 150–200 m thick. Faster advance (up to 500 m day⁻¹) formed a thinner (10–20 m) lava flow on the slopes outside the caldera where the ice was 60–100 m thick. This subglacial lava flow was emplaced along meltwater tunnels under ice for the entire 3.2 km of the flow field length and constitutes 90 % of the total lava volume. The remaining 10 % belong to subaerial lava that was emplaced on top of the subglacial lava flow in an

ice-free environment at the end of effusive activity, forming a 2.7 km long a'a lava field. About 45 % of the thermal energy of the subglacial lava was used for ice melting; 4 % was lost with hot water; about 1 % was released to the atmosphere as steam. Heat was mostly released by forced convection of fast-flowing meltwater with heat fluxes of 125–310 kWm⁻².

Keywords Volcano-ice interaction · Glaciovolcanism · heat transfer · Iceland · Lava flow

Introduction

The largely explosive, 39-day-long, sustained eruption in the summit caldera in Eyjafjallajökull in 2010 (14 April–22 May) and its preceding 23-day-long effusive flank eruption at Fimmvörðuháls (20 March–12 April) offered an opportunity to study several aspects of lava-ice interaction. Some of these aspects have been reported in earlier publications, including magma-ice interaction as revealed by airborne high resolution synthetic aperture radar (SAR) (Magnússon et al. 2012) and the emplacement of the Fimmvörðuháls basaltic lava onto snow (Edwards et al. 2012). Here, we analyse the subglacial emplacement of a 3.2-km-long lava flow field formed in the period 20 April–4 May. We focus on the advance of the lava flow under the glacier ice within the northern part of the summit caldera and subsequent advance down the path of the Gígjökull outlet glacier. The course of events was documented by frequent observation flights, where SAR images were acquired to map out craters, ice cauldrons and lava surfaces. These data are supplemented by videos and still images in the visual and infrared spectrum as well as close inspection of the lava shortly after the eruption ended and during field visits in August 2011 and August 2012. We describe the lava-ice-water interaction during emplacement of the lava flow within the summit caldera and, in

Editorial responsibility: K.V. Cashman

✉ Björn Oddsson
bjornoddsson@gmail.com

- ¹ Nordvulk, Institute of Earth Sciences, University of Iceland, Sturlugata 7, IS-101 Reykjavík, Iceland
- ² Department of Civil Protection and Emergency Management, National Commissioner of the Icelandic Police, Skúlagata 21, IS101 Reykjavík, Iceland
- ³ Department of Earth Sciences, Dickinson College, Carlisle, PA 17013, USA
- ⁴ Faculty of Earth Sciences, University of Iceland, Askja, Sturlugata 7, 101 Reykjavík, Iceland
- ⁵ Icelandic Meteorological Office, Bústaðavegur 9, IS-150 Reykjavík, Iceland

the Gígjökull outlet glacier, establish a thermal model for the system that describes as accurately as possible the heat transfer mechanisms involved and construct a conceptual model for the emplacement of the lava field.

Background

In Iceland, volcanic eruptions beneath glaciers and at ice-covered volcanoes are common (e.g. Larsen 2002; Gudmundsson 2005; Jakobsson and Gudmundsson 2008 and references therein). These eruptions pose a high risk to communities in the vicinity of volcanoes, mainly because of jökulhlaups (flash floods) caused by rapid ice melting (Gudmundsson et al. 2008; Tuffen 2010; Edwards et al. 2015a). Because of this, glaciovolcanism has been studied in Iceland both for historical eruptions (e.g. Gudmundsson et al. 1997, 2004; Gudmundsson 2005; Edwards et al. 2012; Gudmundsson et al. 2012) and for prehistoric eruptions (Höskuldsson et al. 2006; Stevenson et al., 2006; McGarvie 2009; Pollock et al. 2014; Schopka et al. 2006; Tuffen et al. 2008; Stevenson et al. 2011).

Volcanic eruptions at ice-covered stratovolcanoes occur globally, including in North and South America, Kamchatka, New Zealand and the Antarctic. Rapid ice melting during these eruptions can be caused by the emplacement of hot volcanic material onto ice and snow-covered slopes (e.g. dome collapses, pyroclastic flows, pyroclastic falls) that can produce swift outburst floods and lahars (Major and Newhall 1989;

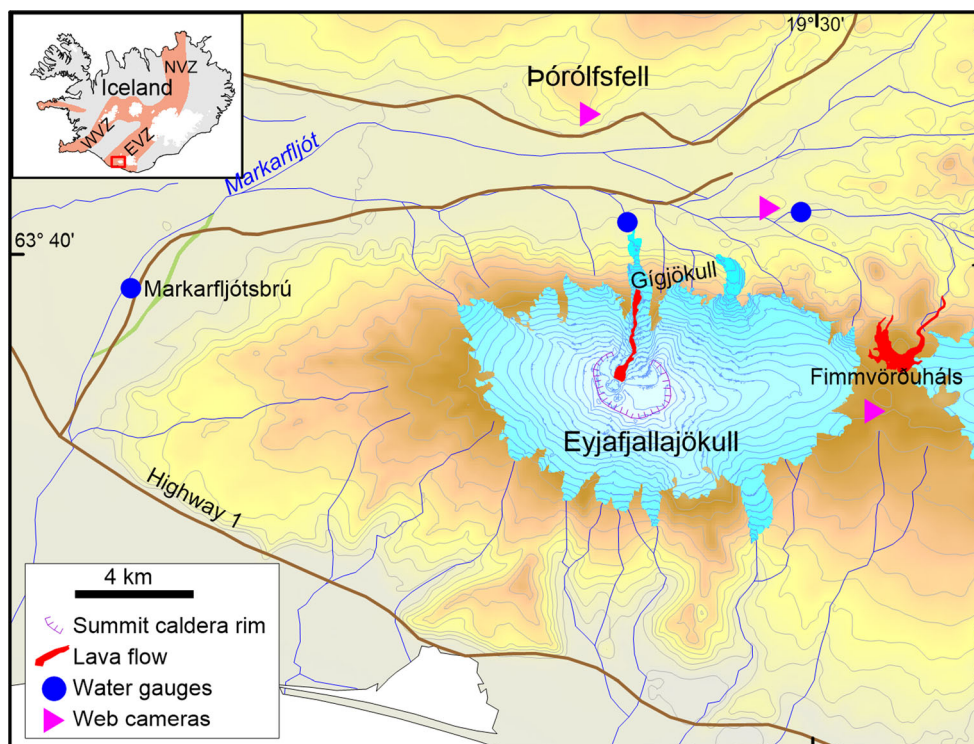
Pierson et al. 1990; Belousov et al. 2011; Waythomas 2014; Delgado-Granados et al. 2015). The potential for disaster from such events was tragically demonstrated by the 1985 eruption of Nevado del Ruiz, where more than 20,000 people in the town of Armero, Columbia, lost their lives in a lahar generated by a relatively small eruption onto the volcano's ice-covered summit (e.g. Pierson et al. 1990; Witham 2005). At some ice-covered stratovolcanoes, historical effusive eruptions have also produced meltwater floods when lava interacted with ice and snow (Major and Newhall 1989) including several examples at Chilean volcanoes (Naranjo et al. 1993; Moreno and Fuentealba 1994; Naranjo and Moreno 2004).

As far as the authors are aware, the work presented here is to date the most comprehensive real-time set of observations yet published on a lava field erupted into a subglacial environment.

Geological setting

Eyjafjallajökull is an ice-capped stratovolcano located near the southern sector of the Eastern Volcanic Zone (Fig. 1). It is elongated east-west, rising to 1650 m above sea level (asl) from a base at 20–200 m asl. The summit of the volcano is covered by an 80-km² ice cap and contains an ice-filled summit caldera that is about 2.5 km in diameter and has a maximum ice thickness of 400 m in the eastern part but about 200 m in the western part (where the 2010 eruption was

Fig. 1 Location of Eyjafjallajökull and the study area, marked with a *rectangle* on the Iceland map. The volcanic zones are labeled Western Volcanic Zone (WVZ), Eastern Volcanic Zone (EVZ) and Northern Volcanic Zone (NVZ)



located). On the slopes outside of the caldera, the ice thickness is typically less than 100 m (Strachan 2001; Magnússon et al. 2012). The caldera wall is breached on the north side, where ice in the caldera flows into the Gígjökull outlet glacier through an 800-m-wide gap (Figs. 1 and 2). Prior to the 2010 eruption, the ice elevation at the northern caldera margin near the head of the Gígjökull outlet glacier was about 1400 m asl. The outlet glacier cascades downwards from the caldera with an average slope of 14° from 1400 to 800 m asl; between 800 and 200 m, it becomes considerably steeper (up to 26°). Prior to the 2010 eruption, the outlet glacier terminated in the Gígjökull proglacial lagoon (Fig. 2).

The 2010 Eyjafjallajökull eruption

Before 2010, Eyjafjallajökull had erupted at least four times in the last 1500 years: ca. 500, 920, 1612 and 1821–23 CE (Larsen et al., 1999; Gudmundsson 2005; Óskarsson 2009). The 2010 eruption in Eyjafjallajökull was preceded by seismicity and ground inflation in 1994, 1999 and 2009 related to intrusive activity (Sturkell and Sigmundsson 2003; Pedersen and Sigmundsson 2006, Sigmundsson et al. 2010). When the rate of seismicity and uplift increased in January 2010, the civil protection authorities raised the alert level for the volcano. The activity intensified significantly in March (Sigmundsson et al. 2010), and on 20 March, a small basaltic effusive fissure eruption started at Fimmvörðuháls, on the northeast flank of Eyjafjallajökull, 9 km to the east of the summit caldera (Fig. 1). This flank eruption terminated on 12 April and produced a series of small lava flows that covered an area of 1.3 km^2 and had a total volume of 0.02 km^3 (Edwards et al. 2012). In the evening of 13 April, an intense swarm of earthquakes started beneath the summit caldera and a subglacial eruption started at about 01:15 GMT on the morning of 14 April. A white eruption plume was visible at 06:00 when the eruption broke through the ice cover (Gudmundsson et al. 2012; Magnússon et al. 2012). Due to the threat of

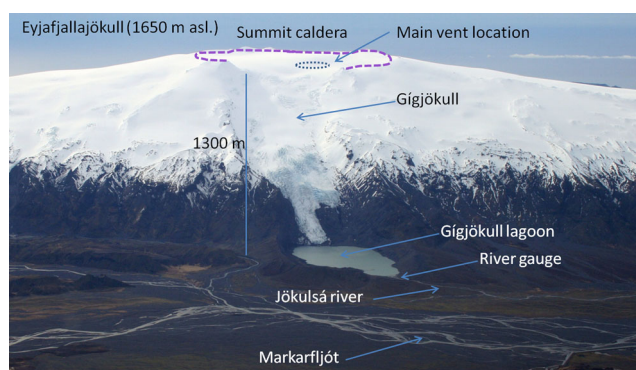


Fig. 2 North side of Eyjafjallajökull on 19 March 2010 prior to the eruption

jökulhlaups from the melting of ice in the summit region, ca. 800 people living nearby were evacuated. The eruption was explosive from 14 to 18 April (phase 1), supporting plumes rising to 5–10 km asl, but by 18 April, the vigour of the eruption was much reduced, demarcating the onset of phase 2 (Guðmundsson et al. 2012; Fig. 3). While the explosive activity continued, its intensity weakened and plume heights decreased to 3–5 km. During phase 2, a lava flow advanced 3.2 km down into Gígjökull outlet glacier. The formation of this lava field is the subject of this paper. The intensity of the explosive activity picked up again around 5 May and remained at higher levels until 17 May, with plumes typically rising to 6–8 km asl height (phase 3). A fourth and final declining phase of continuous activity began on 18 May and ended with eventual cessation of the explosive activity on 22 May.

Methods

The eruption in Eyjafjallajökull was monitored and recorded in a variety of ways: Aircraft-based synthetic aperture radar (SAR), other airborne observations (visual and infra-red imaging), satellite imaging, tephra sampling, seismicity, web cameras and river measurements (Fig. 1) (e.g. Arason et al. 2011; Marzano et al. 2011; Gudmundsson et al. 2012; Magnússon et al. 2012). In this paper, we present results and

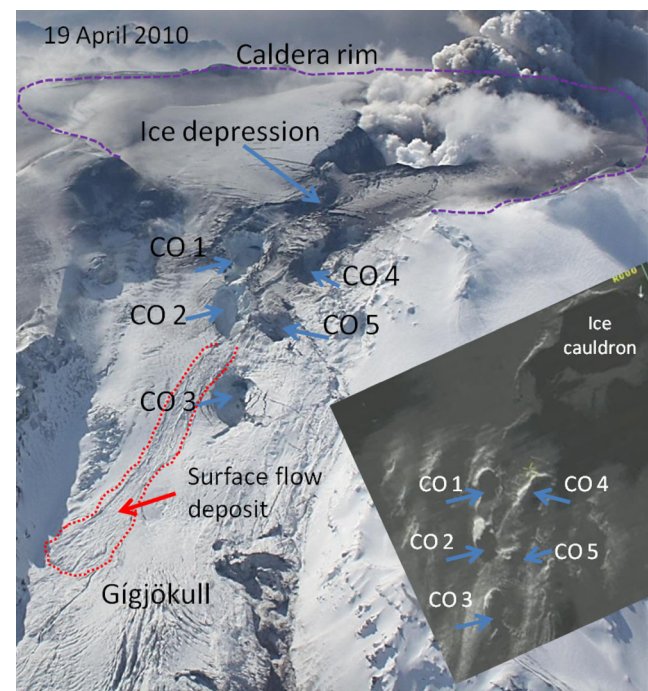


Fig. 3 Aerial photograph taken looking towards the south and synthetic aperture radar (SAR) image from 19 April 2010. Channel openings (CO), which are labelled from 1–5, formed during a jökulhlaup that occurred in the first days of the eruption. A flow comprising meltwater and volcanic clasts travelled partly on the surface of the glacier (red dotted line)

analyses based on mainly visual and aircraft observations during the 15 days of the emplacement of the 3.2 km lava flow.

Definitions

We use the term *caldera* to refer to the summit caldera of Eyjafjallajökull (Fig. 2) and *vent* to describe the exit point of magma from bedrock to the base of ice. *Ice cauldron* is the steep-walled depression melted in the ~200-m-thick ice above the *vent* within the caldera (Figs. 3 and 5). *Cinder cone* is the cone-shaped landform built inside the ice cauldron around the vent (Fig. 4). *Lava mound* is used for the lava mass that accumulated on the northern flank of the *cinder cone*. A *depression* in the ice forms due to melting of ice at the base. *Ice tunnels* were formed by meltwater at the glacier base, and when the roof of the tunnels melted away, an *ice canyon* formed. The length of the *lava flow* is defined as distance from the cinder cone to the lava front.

Syn-eruption observations

Airborne observations were made almost daily using helicopters and a Dash 8 airplane operated by the Icelandic Coast Guard and small commercial piston-engine airplane. The Dash 8 is equipped with high definition cameras, infrared video recorders, side scan radar and, most importantly, a SAR (Magnússon et al. 2012) that was operated from a distance of 15–90 km at an altitude of 4–5 km asl and for which cloud cover, steam and ash plumes are transparent. In the first hours and days of the eruption, the SAR was used to record rapid ice melting that formed ice cauldrons within the summit caldera, as well as subsequent changes in their geometry (Magnússon et al. 2012). During the lava effusion phase of 18 April–4 May, changes related to ice surface subsidence and the growth of the lava field were monitored by SAR.

Post-eruption observations

The lava field in Gígjökull was visited in August 2011 and August 2012. It was confined on the east and west by ice walls forming an ice canyon. Textural and morphological variations of the lava were documented to identify possible evidence of lava-ice interaction. Field mapping also enabled cross-checking of the aerial and satellite observations. Eyjafjallajökull was mapped with an airborne LiDAR on August 12, 2010 (Jóhannesson et al. 2013). The density of the LiDAR point clouds allows interpolation of a regular elevation grid with a 2×2 m cell size and vertical accuracy of <0.5 m (Jóhannesson et al. 2011). The LiDAR map thus provides details of the topography, including the lava flow

surface, crevasse patterns and the various depressions and features in the glacier. This accurate digital elevation model (DEM) allowed detailed cross sections to be constructed of the lava field, accurate calculations of areas and provided constraints for volume estimates.

Observations

Emplacement of the lava flow field and course of events

During the first 2 days of the eruption (14–15 April), ice cauldrons with vertical walls formed around the active vents in the western part of the ice-filled summit caldera where the ice was c. 200 m thick. Water and pyroclasts accumulated in these cauldrons and were episodically flushed in hyperconcentrated jökulhlaups down the northern flank of Eyjafjallajökull. The eruption occurred in late winter, at a time when the glacier's subglacial drainage system from the previous summer was sealed or very inefficient (Magnússon et al. 2012). As a result, rapid formation of meltwater produced high water pressures at the glacier base as well as new pathways. As a result, five channel openings (CO1–CO5) formed in the glacier (Fig. 3), with water escaping and partly flowing supraglacially down the outlet glacier. The channel openings formed in areas with pre-existing crevasses above bedrock undulations. Thus, the meltwater exploited weaknesses in the ice to accommodate the high basal pressures (Fig. 4; Magnússon et al. 2012).

The course of events during phase 2, when the lava field was being emplaced, is summarized in Table 1 and Figs. 3, 4, 5 and 6. On 19 April, an intense, thick white steam plume, apparently free of tephra, was first detected, rising in the northern part of the ice cauldron surrounding the active vent. This was interpreted as lava-ice interaction involving steam formation without evidence of significant magma fragmentation. At this time, meltwater discharge from Gígjökull also started to increase gradually (Fig. 6). From 21 April to 24 April, a depression in the ice north of the active vent gradually grew deeper until a 50 m deep trench that measured $500 \text{ m} \times 500 \text{ m}$ had formed where the ice had previously been 150–200 m thick. No breach in the visible cinder cone wall was observed—apparently, the lava flowed under the cinder cone rim. The pattern of crevassing and ice subsidence indicates that the lava flow reached the northern caldera margin on 29 April. Initially, the average lava advance rate is estimated $<100 \text{ m day}^{-1}$. On 30 April, surface features of the lava flow were first observed in the ice canyon on SAR images; these features being clearly distinct from the ice as a bright surface that indicated a high degree of that surface roughness. These observations confirmed the existence of an active lava flow advancing down the slopes. During this time, steam rose

from crevasses in the glacier at progressively greater distance from vent and was followed by collapse/melting of ice above the tunnels where the lava flowed; eventually, this

process formed a fully open ice canyon. On 1 May, the ice canyon stretched half way down the glacier and intensive steam generation from the whole canyon (Fig. 5d). Lava

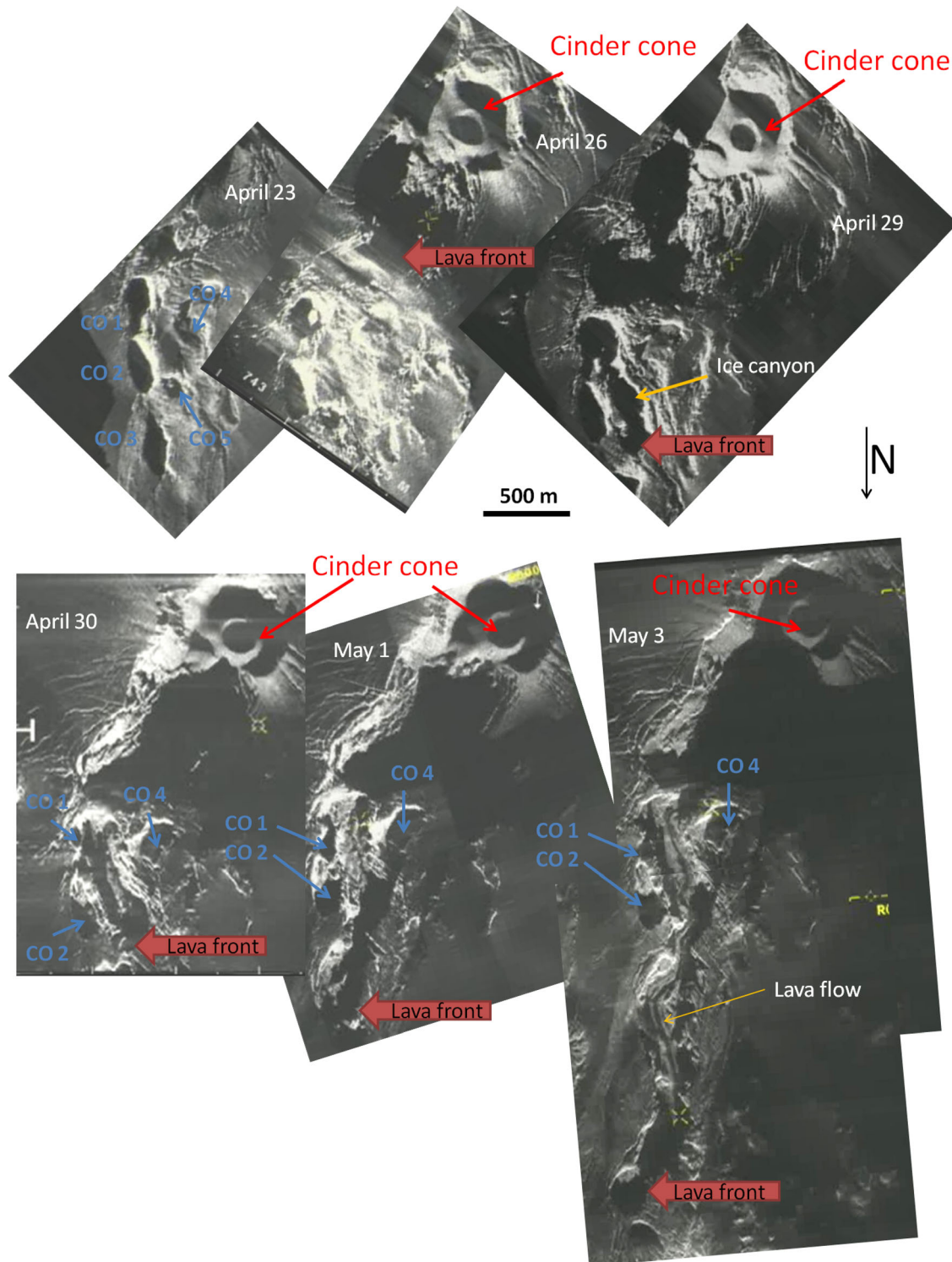


Fig. 4 Synthetic aperture radar (SAR) images show changes in the glacier morphology during the advance of the lava flow. Channel openings (CO 1–CO 5) are marked with blue while the estimated position of the lava front is marked with red arrows. The lava front was

estimated from visual observation and indicated by a dense steam plume. SAR images were used to identify the migration of the lava and were not affected by steam and clouds which obscured the visibility

Table 1 Observations from flights and web cameras on April 20–May 4

Date	Observation
April 20	A narrow depression over the meltwater path of the jökulhlaups north from the vent area was clearly visible but very little other subsidence of the ice had occurred (Fig. 4). Steam generation was limited.
April 21	Steam was observed rising from the north sides of the west cauldron (Fig. 5) in the morning, and in the afternoon, a dense white eruption plume rose straight up from the summit up to 3 km asl. Supraglacial water came from the lowermost channel opening (CO5) in 1300 m asl. Meltwater flowed partly on the surface of the glacier, around the mid-section (1300–2500, 900–600 m asl) (Fig. 5). Flowing water was observed in some of the channel openings. At places, the pathways of water were blocked leading to temporary water accumulation in the channel openings. No steam was observed in channel openings. Continuous low discharge of meltwater spread out on the delta covering the area of the former lake Gígjökulsón.
April 23	SAR images showed that a cinder cone was building up within the ice cauldron (Fig. 4), isolating the vent from the surrounding ice. A lava mound was seen on the northern slopes of the cinder cone. No changes in channel openings were observed.
April 24	The bottom of the depression since April 20 was melted away and steam rose from a 500 m × 100 m area within the depression, reaching from the cinder cone (Fig. 5). Steam plume rose to the summit elevation of Eyjafjallajökull (1.6–1.7 km asl, 200–300 m over source). No steam was observed from the channel openings in Gígjökull.
April 26	SAR images (Fig. 4) revealed that the rims of the cinder cone continued to grow and fill up the volume within the ice cauldron. The lava mound on the northern slopes of the cinder cone it had grown since April 23.
April 27	Ice had completely melted above the lava out to 1100 m and had merged with CO 1 forming a continuous ice canyon. A steam plume rose to a few hundred metres at 500 m (Fig. 5). FLIR images revealed >400 °C on the cinder cone and on the lava surface at the bottom of the ice canyon, where visible between steam clouds. Fumes rose from channel opening CO 5 and a new hole in the ice between CO 4 and CO 5 with concentric subsidence around it. This suggested warm meltwater draining after temporary storage at this location.
April 28	Fumes rose temporarily from CO 4 and CO 5 in association with small flash floods on the delta in front of Gígjökull. The largest such flood occurred at 11:28. As the water reached the delta, it was still warm, since fumes rose from the floodwater. A constant steam plume was seen in the lower most part of the glacier (CO 5).
April 29	The size of the lava mound increased since April 26 (Fig. 4). The ice canyon extended northwards, merged with the upper most channels opening (CO 1), passed west of CO 2 and reached to CO 5. A part of the SAR images show in great detail the surface of the lower part of Gígjökull. No changes had occurred since the floods on April 14–16.
April 30	Surface features of the lava were visible for the first time on SAR images (Fig. 4). The lava was observed as flowing through the ice canyon to the west of the eastern channel openings (CO 1–CO 3). The lava was 1700 m long. In the evening (21:00), web cameras showed thick, continuous steam plume rising from the whole ice canyon.
May 1	Ice canyon reached down to the mid-section of the glacier at 2100 m (900 m asl) (Fig. 4). Steam plume rising from the ice canyon north of the crater was denser than before and was generated from the whole ice canyon (Fig. 5), largely obscuring its base. No steam rose up from CO 2 and CO 3. The glacier was heavily crevassed on both sides of the ice canyon. Large, seemingly unstable blocks of ice marked the margins of the tunnel in places.
May 2	A continuous steam plume was generated from the ice canyon during the day.
May 3	The ice canyon stretched all the way from the crater down to length 3050 m, at an altitude of 800 m. Surface features of the lava flow were visible on SAR images, showing levies to the sides and a trench in the centre (Fig. 4).
May 4	The flow had reach 3200 m in length and could be split into an upper flow and a lower flow, with the upper flow terminating in a distinct front, some 500 m south (unslope) of the margin of the lower flow. Apparently, the upper lava had flowed down the already formed ice canyon, having limited contact with ice. The lava front was 350 m from reaching the upper part of the delta in front of Gígjökull. Steam rose only from the lower end of the ice canyon, as well as some more fumes occasionally rising from the upper parts of the ice canyon.

propagated outside the caldera between 30 April and May 4 with the fastest advance and open ice canyon formation observed between 2 May and 4 May. During this period, the lava flow advanced at ≤ 500 m day⁻¹ reaching its maximum length of 3.2 km from its source. At the same time, meltwater discharge increased from 80 to 300 m³ s⁻¹ followed by an abrupt drop to 50 m³ s⁻¹ on 5 May (Fig. 6). At no time was lava observed flowing on top of ice, apparently all lava advance occurred at the glacier bed.

At the end of the eruption, the lowermost part of the lava flow field was covered by fragmented glacier ice. During the

summer and autumn after the eruption, the ice melted away and the lava field was exposed (Fig. 7). These areas were explored in the summer of 2011 and 2012.

Field observations of lava characteristics

The morphology of the lava observed on ground in the lowermost 800 m of the lava flow defines two distinct types (Fig. 8a), one of which has characteristics of a lava flow that has interacted with ice (Fig. 8c) and water, and the other shows no water or ice interaction (Fig. 8b).

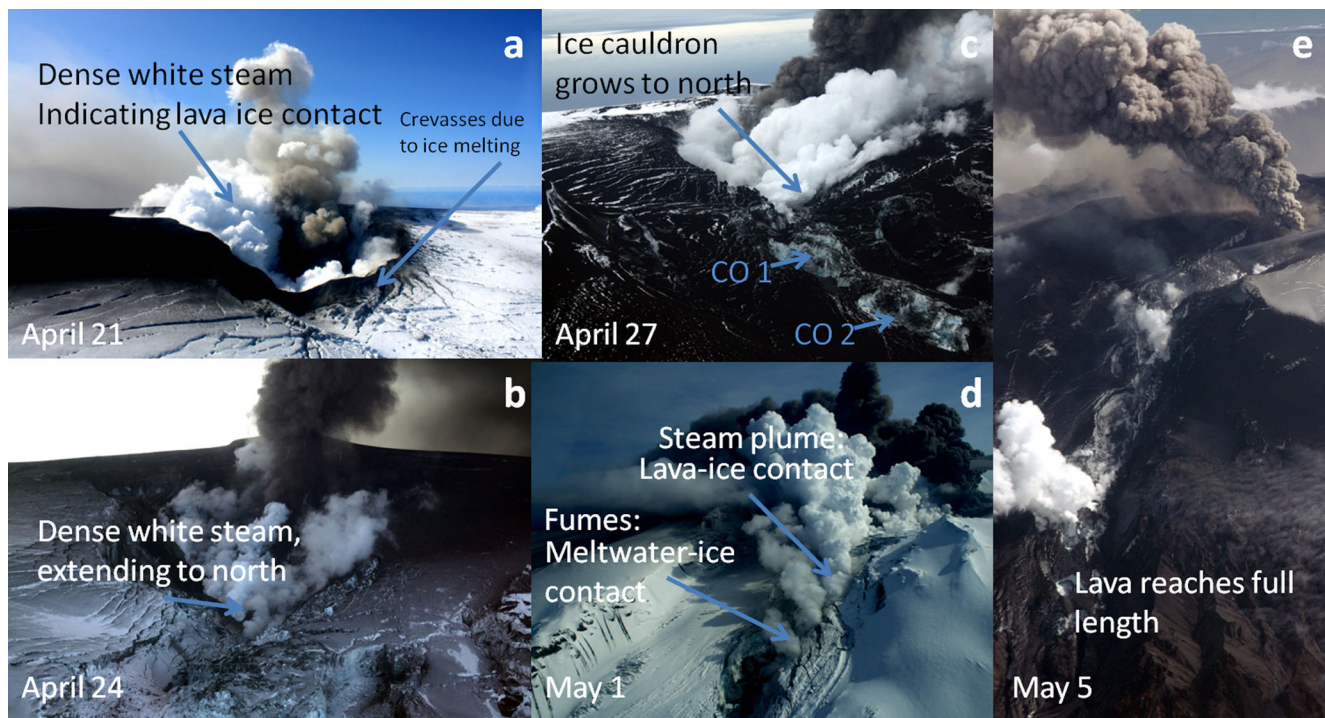


Fig. 5 Advance of lava downslope from summit (April 21, April 24, April 27, May 1 and May 5). **a** On April 21, lava started to flow down the northern flank of the cinder cone building up within the northern-most ice cauldron. A thick white steam plume indicated direct lava/ice contact. **b** The lava mound continued to grow, and on April 24, it started to advance to the north, widening the ice cauldron to the north. **c** By April 27, the deforming ice in the depression north of the lava mound was completely melted, allowing the lava to flow subaerially for the first

300 m away from the centre of the lava mound. **d** On May 1, the lava advanced faster because it encountered previously melted tunnels and a steeper bedrock surface. The upper part was subaerial while the lower part flowed subglacially in tunnels, allowing direct lava-ice and water interaction. **e** After advancing faster from April 29–May 4, the lava reached its maximum length of 3200 m, measured from the outer rim of the cinder cone, on May 5. Thick white steam rises from the lava front while an ash-rich plume rises from the cinder cone

Subglacial lava

The lava furthest (3.2 km) from the caldera comprises mostly individual lobes that partly overlap each other, being emplaced until May 4. The surface is covered by breccia and tephra, and the lava has vesicular tops and dense, vitric cores. In several locations, remnants of ice tunnels (ice arches) were found 2.8–3.2 km from the vent

area. In these tunnels, lava tongues on the order of few metres wide are frequently covered by water-transported sediments (Fig. 8e). These lavas are interpreted as having been emplaced subglacially at the glacier-bedrock interface. The abundance of vitric material, lack of oxidation and locations within ice tunnels (preserved locally) are consistent with lava advance through meltwater tunnels, largely filled by meltwater.

Fig. 6 Discharge of meltwater from Gígjökull and temperature measured at Markarfljótsbrú, 18 km downstream from Gígjökull in the period from April 20 to May 7

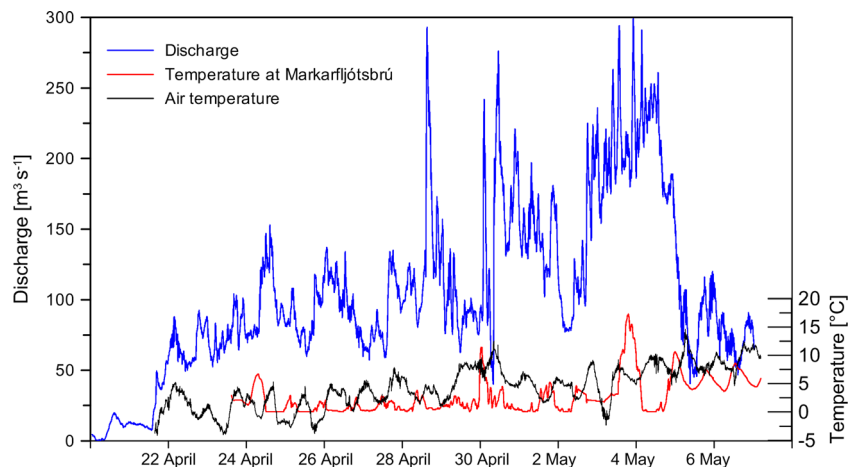
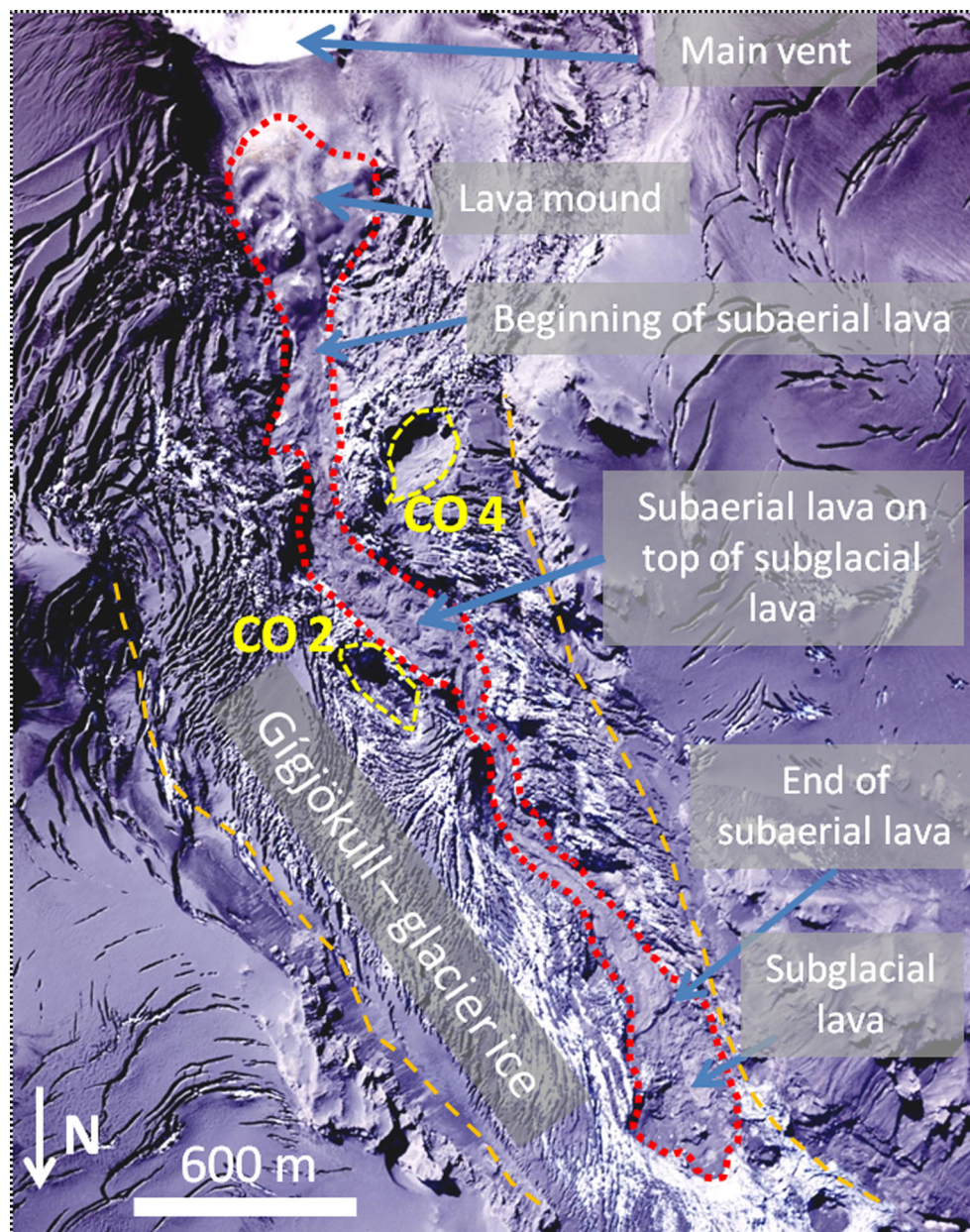


Fig. 7 Satellite image showing the outlines of the lava (red, dotted line). East and west margins of Gígjökull glacier are marked with dashed orange line and channel openings 2 and 4 with a broken yellow line



Subaerial lava

Approximately 500 m upstream from the end of the lava field, a steep, blocky lava front rests on top of the lava mounds interpreted as emplaced subglacially. The upper blocky lava has a typical subaerial lava morphology and is covered by partly oxidized blocks (clinker) and minor tephra cover on its surface (Fig. 8d). The subaerial lava flow is typified by an open lava channel bounded by well-developed levees. It was emplaced after the bulk of the ice melting took place in Gígjökull. At the time of its emplacement, the ice canyon had already formed and the subaerial lava flow advanced with limited interaction with water and ice for 2.7 km downslope from the caldera margin. After its emplacement, ice fragments

occasionally fell onto the solidified surface causing small steam plumes.

Estimates of lava area and volume

The lava flow is easily delineated on the LiDAR map from August 2010 (Fig. 9), from which its area is determined to be $0.55 \pm 0.10 \text{ km}^2$. In order to estimate the average flow field thickness, a set of cross sections was extracted from the LiDAR map at 200 m intervals along the entire flow field. Maps of the subglacial bedrock topography before the eruption are not available. However, after the eruption, the bedrock was visible in several places along the ice canyon. The surface slope of the glacier (Fig. 10) also provides constraints on the

Fig. 8 **a** The lowest part of the lava field where the subaerial lava flow stops and the subglacial lava is visible. **b, d** The subaerial lava has blocky surface and less tephra coverage. **c** The subglacial lava flow is lobate with breccias on top and thicker tephra cover. **e** Ice arch, remnants from ice tunnels. Subglacial lava is outlined by red dotted line. The lava is partly covered by water-transported sediments



pre-eruption topography. We assume a glacier relating basal shear stress (τ_0), ice thickness (H) and slope (α). Here, the density of the glacier is ρ_{ice} (900 kgm^3), g is gravitational acceleration (9.8 ms^{-2}) and $f'(0.75)$ is the ratio between driving stress and basal stress estimated from the width of the glacier (Paterson 1994):

$$H = \frac{\tau_0}{f' \rho_{ice} g \sin(\alpha)} \tag{1}$$

Equation 1 can be used to estimate the thickness of the glacier and therefore also the bedrock elevation. Together with observations in the field, we calculate a lava volume (V_{lava}) of $2.5 \pm 0.6 \cdot 10^7 \text{ m}^3$. About three quarters of this volume resides inside the summit caldera ($1.8 \pm 0.5 \cdot 10^7 \text{ m}^3$) and one quarter ($0.7 \pm 0.2 \cdot 10^7 \text{ m}^3$) forms a much thinner lava flow along the path of Gígjökull, outside the summit caldera. The entire lava field within the summit caldera is considered to be subglacial, as is most of the lava in Gígjökull, yielding a total

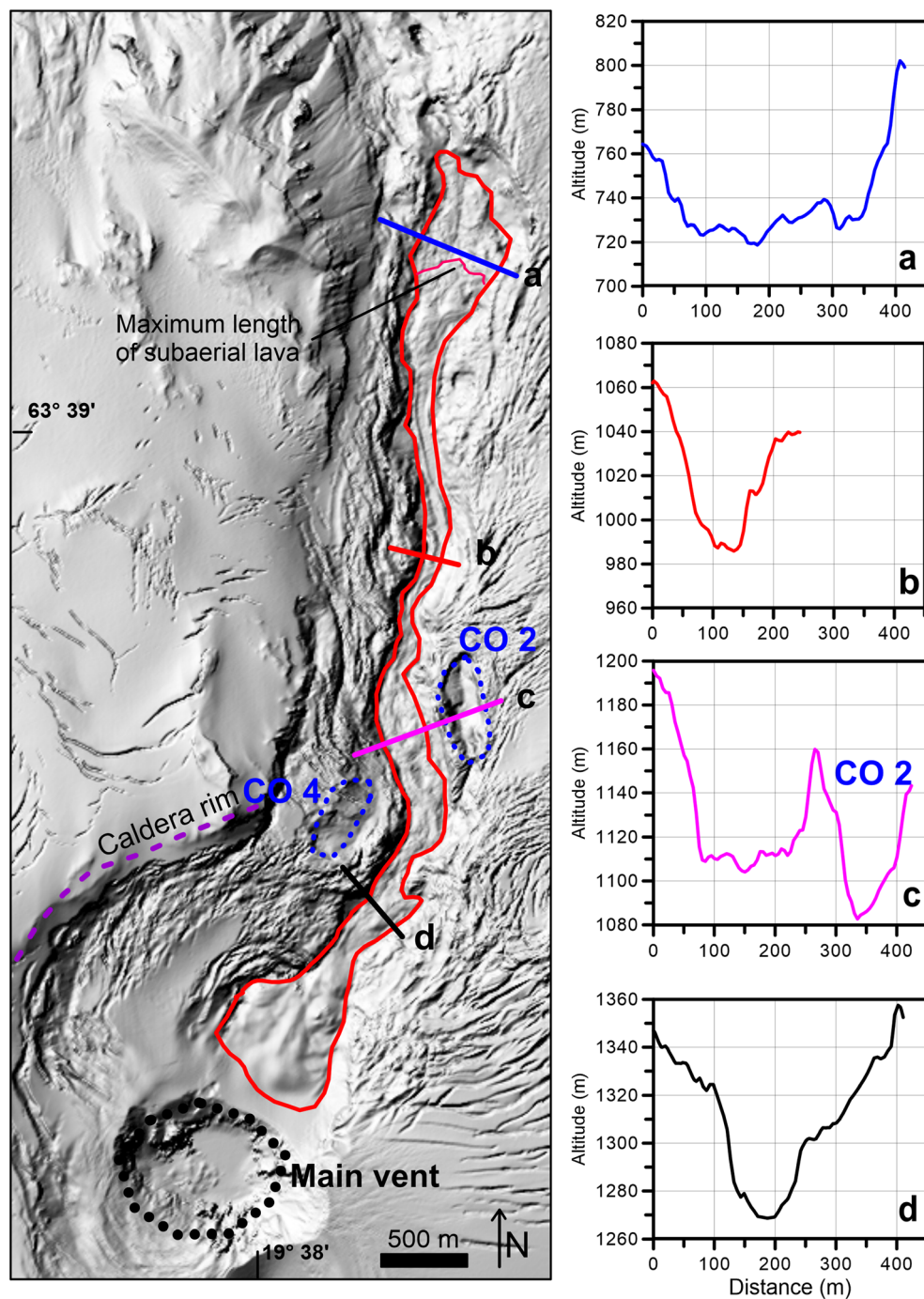
subglacial volume of $2.3 \pm 0.6 \cdot 10^7 \text{ m}^3$ and $0.2 \cdot 10^7 \text{ m}^3$ for the subaerial lava.

Thermal history of the lava-ice-water system

Controlling modes of heat transfer

Heat transfer in a subglacial environment, where ice, water and lava interact, is controlled by thermal convection and advection of heat by flowing water which is about two orders of magnitude more effective as a coolant than air under conditions of both free and forced convection (e.g. Çengel and Boles, 2006). Another factor that contributes to heat transfer is steam generation, where heat can be lost to the atmosphere, as well as heat conducting to the underlying bedrock (Wooster et al. 1997). In general, heat transfer from lava to its surroundings involves a complex mixture of processes including radiation, convection and conduction. Where lava is submerged in

Fig. 9 LiDAR map of Eyjafjallajökull measured in August 2010 (Jóhannesson et al. 2013) showing the summit caldera of Eyjafjallajökull, craters formed during the 2010 eruption and the outlet glacier and Gígjökull, where lava (marked with green line) flowed during the eruption. The map has resolution of 2×2 m. Lines labelled a to d correspond to topographic profiles shown to the right



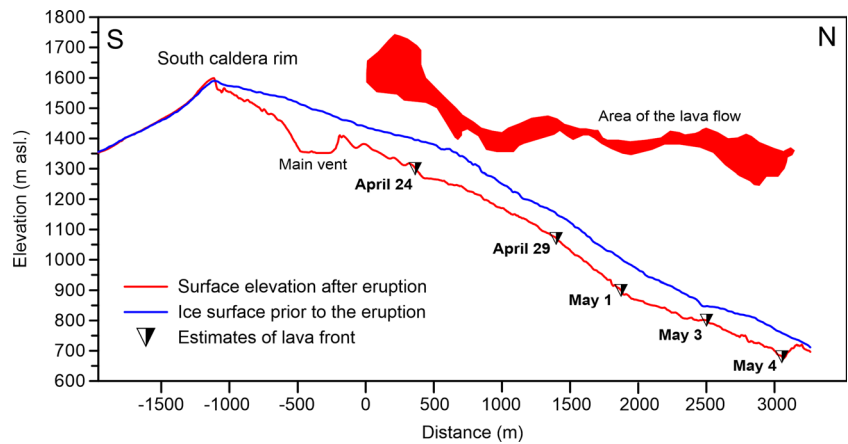
water, the lava surface is rapidly cooled with heat transfer controlled by conduction through a rapidly formed lava crust, when water flows on top, rapid heat transfer is aided by forced convection in the water. Radiation to the overlying water can be ignored as lava surface temperatures are expected to drop in a matter of seconds from magmatic to values closer to that of the surrounding water (Moore, 1975). As in the flow of lava on the surface of the Earth, the insulating effects of the rapidly formed lava crust are essential for keeping the lava hot and fluid and allowing it to continue downslope (e.g. Keszthelyi

et al. 2006). After an eruption, residual heat retained within the lava is gradually released during cooling.

Energy balance for subglacial lava flow

During the 2010 Eyjafjallajökull eruption, the mass of lava erupted and the mass of ice melted can be estimated with reasonable accuracy (about 20 % uncertainty) and the temperature of the meltwater released from the glacier is known. Thus, individual components of the system's heat balance can be

Fig. 10 South–North cross-section over the summit, main vent area and Gígjökull glacier showing the altitude of the glacier surface prior to the eruption. The post-eruptive section from the main vent down to length of 3200 m is the lava surface



estimated. The results enable comparison of estimates of the total thermal energy of the lava to the heat consumed by melting ice, heating of meltwater and steam generation. We also consider the implications for residual heat and estimate the rates at which heat was lost from the lava as thermal energy.

Here, a simple energy balance is applied to estimate the average heat transfer rates from observations and field measurements making use of heat transfer applications to these settings (Höskuldsson and Sparks 1997; Wooster et al. 1997; Wilson and Head 2002; Gudmundsson 2003; Wilson and Head 2007).

Energy balance of the lava-ice-meltwater-steam system

The overall heat balance for the system during emplacement of the subglacial lava flow can be written as follows:

$$E_{\text{lava}} = E_{\text{ice}} + E_{\text{water}} + E_{\text{steam}} + E_{\text{res}}, \tag{2}$$

where E_{lava} is the total available thermal energy from the erupted lava, E_{ice} is energy spent melting ice, E_{water} is energy extracted from the lava by meltwater and not transferred to the ice, E_{steam} is energy used for steam generation into the atmosphere and E_{res} is the residual energy stored in the lava field after lava emplacement came to a halt. Energy transferred to the bedrock via conduction in the time frame of the emplacement of the lava is negligible and therefore not included in the overall heat balance. Heat lost with radiation to the atmosphere is also considered to be negligible for the subglacial lava flow.

Initial heat in the lava flow

The amount of thermal energy available from the lava by cooling (sensible heat) and solidification (latent heat) is obtained from

$$E_{\text{lava}} = V_{\text{lava}} \rho_{\text{lava}} [L_{\text{lava}} + c_{p,\text{lava}}(T_i - T_0)] \tag{3}$$

where V_{lava} is the volume of subglacially erupted lava flow ($2.3 \pm 0.6 \cdot 10^7 \text{ m}^3$), ρ_{lava} is density (2400 kg m^{-3} ; Gudmundsson et al. 2012), L_{lava} is the latent heat of fusion ($3.7 \cdot 10^5 \text{ J kg}^{-1}$), $c_{p,\text{lava}}$ is the lava heat capacity ($1.0 \cdot 10^3 \text{ J kg}^{-1} \text{ K}^{-1}$; Oddsson et al. 2016), T_i is the initial (magmatic) temperature (1300 K, Keiding and Sigmarsson 2012) and T_0 is the ambient temperature (taken to be the freezing point of water, $T_0 = 273 \text{ K}$). We constrain E_{res} by estimating the first three terms on the right hand side of eq. (2) and then use eq. (3) to estimate the total heat available. The difference provides an estimate of E_{res} , which should be lost gradually over a timescale much longer than the duration of lava emplacement. Using eq. (3), the total thermal energy contained in the subglacial lava flow is estimated to be

$$E_{\text{lava}} = 7.8 \pm 2.2 \cdot 10^{16} \text{ J.}$$

Heat consumed for ice melting

The thermal energy required to melt ice can be estimated from

$$E_{\text{ice}} = V_{\text{ice}} \rho_{\text{ice}} L_{\text{ice}} \tag{4}$$

Standard values for ice are used in Eq. (4) with $\rho_{\text{ice}} = 900 \text{ kg m}^{-3}$ and $L_{\text{ice}} = 334 \text{ kJ kg}^{-1}$ (Çengel and Boles, 2006).

Volume of melted ice (V_{ice}) was estimated by calculating the ice loss from digital elevation models (DEM) produced before and after the eruption. Within the summit caldera, the volume of ice melted after 18 April is $6.8 \pm 0.7 \cdot 10^7 \text{ m}^3$ and the volume melted to the north of the summit caldera, in Gígjökull, is $4.6 \pm 0.5 \cdot 10^7 \text{ m}^3$. This gives a total of $1.14 \pm 0.17 \cdot 10^8 \text{ m}^3$ of ice melted due to the advance of the lava, equivalent to $1.05 \pm 0.16 \cdot 10^7 \text{ m}^3$ of water. Thus, E_{ice} is $3.5 \pm 0.5 \cdot 10^{16} \text{ J}$, ~45 % of the total energy.

Heat advected with meltwater beyond glacier margin

The temperature of the meltwater was measured 18 km downstream from Gígjökull. Analysis of the temperature series

(lower curve on Fig. 6) shows diurnal variations until 28 April, suggesting daytime heating over this period. This indicates that atmospheric heat was transferred to the river and that the meltwater issued from Gígjökull at a temperature not significantly above zero. In the period 28 April–5 May, spikes in water temperature ranging from 8° to 17 °C occur when water discharge is 70–300 m³ s⁻¹. This is in line with observations of steaming water emerging from Gígjökull which indicates temperature of significantly above freezing, although no direct temperature measurements were made close to the outlet. At other times (e.g. mid-day 1 May), ice in the water, both at the outlet and by the bridge, 18 km downstream was observed indicating that the meltwater was emerging at ~0 °C. An order of magnitude estimate of energy transport associated with meltwater beyond the ice edge can be made by assuming that the observed peaks in temperature between 28 April and 5 May represent release of meltwater at temperatures two to three times higher than measured at the bridge (8–50 °C), assuming significant cooling of meltwater along the 18 km river path. The volume of water released during these temperature peaks was approximately 2.5·10⁷ m³.

The energy consumed to heat the meltwater can be crudely estimated by summing up the contributions from the six occasions of elevated temperature observed between 28 April and 5 May:

$$E_{\text{water}} = \rho_{\text{water}} c_{p,\text{water}} \sum_{i=1}^6 \left[\int_{t_i}^{t_f} \left(\frac{dV}{dt} \right)_{\text{water}} T(t) dt \right]. \quad (5)$$

Here, (dV/dt)_{water} is discharge in m³ s⁻¹, $T(t)$ is estimated water temperature (2–3 times observed at bridge), t_i is the time of initiation of the temperature anomaly and t_f is the time when it stops and $c_{p,\text{water}}$ is the heat capacity of water (4.187 kJkg⁻¹ K⁻¹). The thermal anomalies occurred on April 28 and 29 and May 2, 3, 4 and 5. E_{water} is then 2–4·10¹⁵ J, an order of magnitude smaller than the energy used for melting ice.

Heat consumed for steam generation

The energy consumed by steam generation is estimated using the empirical relationship between the energy required to generate the plume (Q) and the height of the top of the plume (H) (Morton et al. 1956) in standard atmosphere:

$$H = 46Q^{\frac{1}{4}} \quad (6)$$

H is measured in m and Q in kW . This equation can be solved for Q , as

$$Q = 2.23 \cdot 10^{-7} H^4 \quad (7)$$

A first-order estimate of the magnitude of energy used to generate the steam plume can be made by integrating equation

(7) using records of steam plume height over time (Morton et al. 1956):

$$E_{\text{steam}} = \int_0^t (2.23 \cdot 10^{-7} H^4) dt. \quad (8)$$

The integration is performed over the time when significant steam plumes were generated. Steam generation from the ice canyon was intense for 4 days, 1 May–4 May. As it was only possible to observe the steam plume during the day, the highest plume altitude measured per day was used and assumed to apply over 24-h period. The maximum height is used to obtain an order of magnitude of the upper bound of the energy required for the plume. The steam rose to a maximum of 2.0 ± 0.2 km above the lava field for 2 days and 1.0 ± 0.1 km for the other 2 days. This gives a total $E_{\text{steam}} = 6.5 \cdot 10^{14}$ J for these 4 days, which is two orders of magnitude less than the energy required to melt ice.

Total energy balance

From the energy balance calculations above, we find that the estimated residual energy in the lava field after effusion ceased is

$$\begin{aligned} E_{\text{res}} &= E_{\text{lava}} - (E_{\text{ice}} + E_{\text{water}} + E_{\text{steam}}) \\ &= 7.8 \pm 2.2 \cdot 10^{16} - 3.7 \pm 0.6 \cdot 10^{16} = 4.1 \pm 1.7 \cdot 10^{16} \text{ J} \end{aligned}$$

This result implies that at least 50 % of the initial thermal energy within the lava is extracted from it during emplacement. The remaining 50 % of the energy is stored mostly in the thickest part of the lava in the summit caldera. The lowermost part, where the lava is thinnest and meltwater has good access to the lava field, heat is extracted at a much faster rate.

The importance of meltwater during the emplacement of the lava is twofold: first, it extracts heat from the lava, which could affect the lava's viscosity and physical behaviour (Griffiths 2000), and secondly, it transports the heat down-slope from the location of the lava at any given moment resulting in enlargement of existing subglacial ice tunnels and possibly the creation of new ones, thus allowing the lava to continue its subglacial migration.

Heat flux from lava to ice

Lava in the caldera

A growth of a depression at the surface of the glacier ice was observed while lava was piling up within the caldera and starting to flow subglacially towards the uppermost part of Gígjökull. The surface depression was formed due to heat extracted from the lava. It can be extracted by two principal mechanisms: (1) Via conduction from the upper surface of the lava to the ice, with the resulting meltwater flowing

continuously away from the contact zone. (2) Via infiltration of water into cooling cracks in the lava, where heat is removed and convected away by the water and possibly steam formed in the cracks (Tuffen et al. 2002). This second process may, at least, initially enhance heat transfer and consequently the rate of ice melting.

Heat flux can be estimated using equation 4 to calculate the energy required to melt the observed volume of ice over a known time period. From 21 April–24 April (72 h), $\sim 7.5 \pm 1.9 \cdot 10^6 \text{ m}^3$ volume of ice was melted in a 50 m deep depression and $\sim 500 \text{ m} \times 500 \text{ m}$ in area north of the active vent. This requires $8.9 \pm 2.2 \cdot 10^9 \text{ W}$. The area of the lava emplaced under the depression is estimated from the Lidar map to be $6.1 \pm 0.6 \cdot 10^4 \text{ m}^2$, yielding a heat flux of $150 \pm 25 \text{ kWm}^{-2}$. This is an order of magnitude less than the heat transfer on 14 April when the eruption was entirely explosive, as it melted its way through the overlying ice while the ice cauldrons were forming (Magnússon et al. 2012).

Lava in Gígjökull

The area of the lava flow outside the caldera, $A = 3.0 \pm 0.5 \cdot 10^5 \text{ m}^2$, is used to estimate the heat flux during the propagation of the lava flow down the Gígjökull glacier. The propagation occurred primarily 30 April–4 May (120 h) and during that time ice melting is estimated to have amounted to $7 \cdot 10^7 \text{ m}^3$, or $E_{\text{ice}} = 2 \cdot 10^{16} \text{ J}$. If we assume that the average lava area over this period is half the final ($A/2$), the following expression can be used for heat flux (q):

$$q = \frac{2E}{At}. \quad (9)$$

Applying equation 9 to the 30 April–4 May period, we get a flux $\sim 310 \text{ kWm}^{-2}$. This value is twice that of the caldera lava, perhaps because the steeper slope caused faster lava and meltwater flow, leading to more efficient forced convection. It may also be that this value is on the high side, since tunnel widening by warm meltwater before 30 April may account for a part of the ice volume melted.

Discussion

Conceptual model of the lava emplacement

Based on our observations and thermal considerations, a conceptual model for the emplacement of lava beneath a relatively steeply sloping outlet glacier is presented. We consider that meltwater is the working fluid that transfers heat from the lava and advects heat downslope where it is used in enlarging existing meltwater tunnels and, to a lesser extent, in excavating new tunnels.

The model as it applies to Eyjafjallajökull is presented schematically in Fig. 11. The first stages (Fig. 11a, b) represent the initial part of eruption, which formed ice cauldrons with a mixture of tephra and meltwater. When hydrostatic pressure exceeded the glaciostatic pressure, the mixture exited the cauldrons in high discharge jökulhlaup (Magnússon et al., 2012). The cycle of meltwater accumulation and release was repeated until the production of meltwater slowed or a situation of continuous drainage was established. The jökulhlaups formed a subglacial drainage system that locally was open to the glacier surface where ice tunnel roofs had collapsed. Once the ice cauldron had reached sufficient width and accumulation of tephra against the ice walls had restricted contact between magma and ice, the rate of meltwater was much reduced (Fig. 11c). During this stage, access of water to the vents was reduced and a cinder cone started to build up within the ice cauldron. Coinciding with a drop in magma production rate, the eruption turned partly effusive (Gudmundsson et al. 2012) and lava started to flow outside the northern flank of the cinder cone within the summit caldera, allowing lava-ice interaction and increasing production of meltwater (Fig. 11d). Meltwater drained freely away from the vent area as it was generated, continuing to expand the drainage system and forming a tunnel at the base of Gígjökull outlet glacier that extended to the glacier snout/terminus. The widening of the tunnel was principally thermal and was most pronounced in the first few hundred metres downslope of the lava front but much reduced further away. (Fig. 11e). Lava advanced subglacially down the previously carved meltwater tunnels under Gígjökull and thick, white steam plumes formed where direct interaction was between the lava and the meltwater. The lobate morphology of the subglacial lava flow indicates that it was transported through well-insulated pathways to the leading edge of the flow while still relatively hot and fluid. This was possible due to rapid formation of a coherent (and relatively thick) insulating crust between the molten lava and the overlying meltwater. In addition to the insulating effect, the local bedrock slope affects the rate of advance, but the observations cannot differentiate between this effect and the effect of possible changes in lava discharge. The transfer of heat from the lava was meltwater-enhanced to maintain the ice melting in the tunnels and, eventually, the ice melted away (Fig. 11f). The subaerial lava flow is inferred to have formed when the internal pathway within the subglacial lava flow inside the ice canyon in the upper, steep part of the outlet glacier, just north of the summit caldera margin, was no longer effective. This second lava flow (subaerial) flowed on top of the ice free and relatively dry earlier formed lava. Steam was generated either where ice blocks fell on top of the lava flow or meltwater streams percolated through the top or sides of the lava, but the

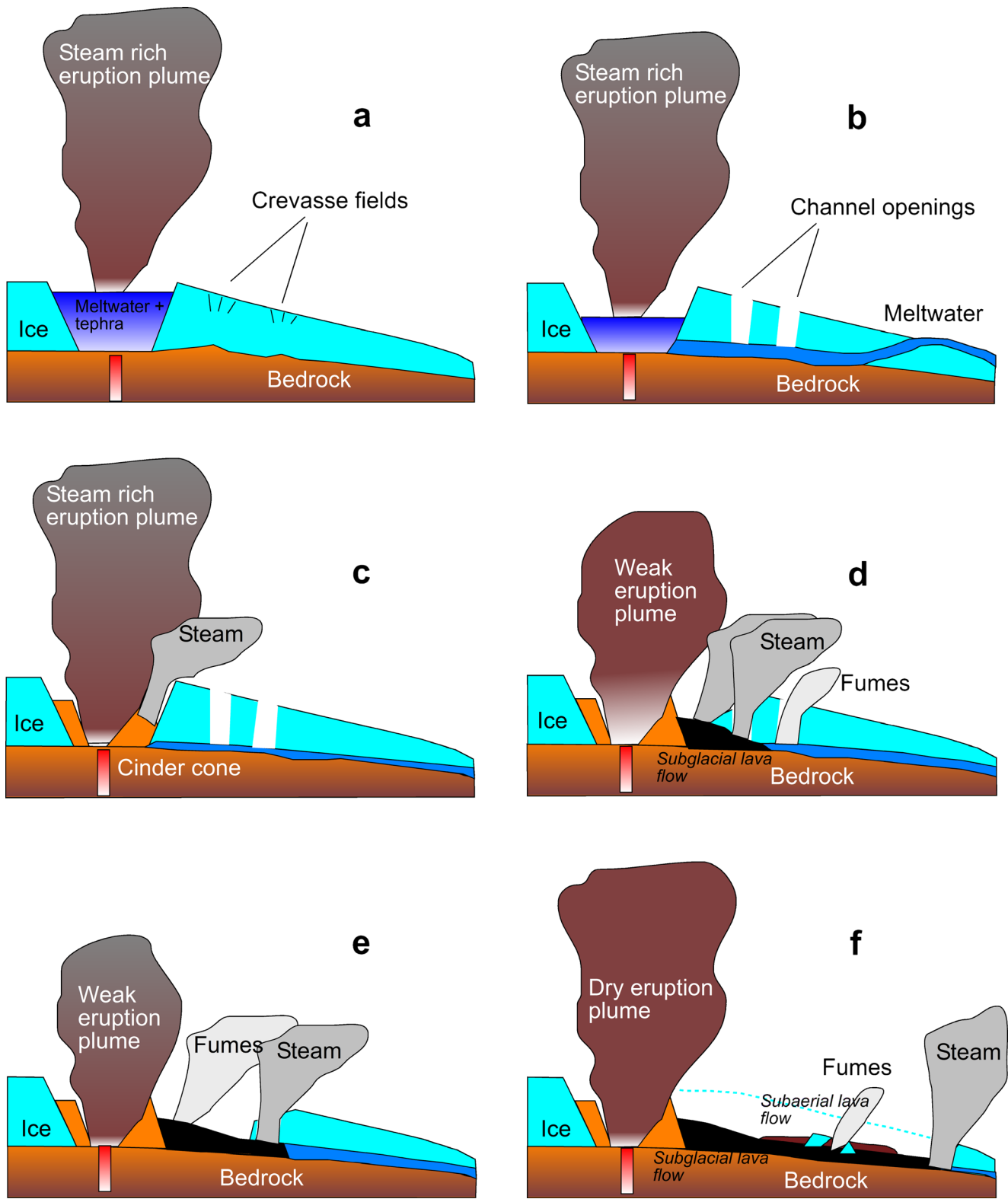


Fig. 11 Emplacement model for the subglacial lava flow in Gígjökull. **a** Phreatomagmatic eruption—water-filled ice cauldron. **b** Water and tephra drained from ice cauldron in a swift jökulhlaup. **c** Ice cauldron water free—cinder cone starts to build up—eruption becomes mixed explosive-effusive. **d** Lava advances under north cinder cone rim

towards north under ice. **e** Lava closest to the cinder cone no longer covered with ice, melting continues and lava front advances under ice towards the outlet glacier. **f** Lava flow has reached its full length, overlying ice mostly melted. Subglacial lava flow partly covered by subaerially erupted lava

fumes formed were miniscule compared to those observed on 1–4 May.

The general scenario for lava effusion at an ice-clad stratovolcano is described by Lescinsky and Fink (2000). Meltwater generated due to lava-ice interaction travels freely downslope through pre-existing englacial and subglacial tunnels. The tunnels are enlarged by thermal and mechanical erosion, allowing for increased discharge and for partial tunnel occupation by lava and syn-eruptive debris. With time and depending on the thickness of the overlying ice, the tunnel roofs are undercut and collapse to form an open canyon and allow meltwater to pond. Lescinsky and Fink (2000) suggested that intense steam indicates direct lava-ice contact; this has been confirmed by close field observations at recent eruptions (e.g. 2010 Fimmvorðuháls (Edwards et al. 2012) and 2012–2013 Tolbachik (Edwards et al. 2015b)). They also suggested that substantial meltwater runoff is produced. This description fits well with the observations and the conceptual model presented here. However, as the emplacement of the subaerial lava flow shows, once confining ice roofs have melted, subsequent lava pulses may record little evidence of their englacial environment and partly conceal the evidence for ice-canyon emplacement.

Eruptive environment

Our work clearly shows that a lava flow with the same rheology erupted within a relatively short time without any break in discharge can result in two distinctive morphologies after it is emplaced and solidified. The largest influence here is the syn-eruptive change in the surrounding environment from one where lava has significant contact with ice and meltwater, to one with limited or no contact with the same. The variable during the eruption is the access and interaction with ice and meltwater. When the ice is melted away in the lava's path leading to cessation of lavameltwater interaction, the lava morphology changes. Even though the lava may still be constrained on both sides by glacial ice 50–100 m thick, the lava morphology may not record the presence of the glacier. This needs to be taken into account where prehistoric subglacial lava fields are recognized. Edwards et al. (2015a) found similar effects for lava erupted beneath snow during the Tolbachik eruption, where lavas erupted beneath snow had distinctly more bulbous morphologies and were more vitric than surrounding subaerial lavas. The present study and that from Tolbachik show that detailed field investigations of lava morphologies may be necessary to identify products from early parts of the eruption when snow/ice was present, which were subsequently obscured by more typical subaerial lava morphologies.

Jökulhlaups

Jökulhlaups are one of the largest hazards associated with volcanic eruptions in Iceland. The Eyjafjallajökull eruption started subglacially under approximately 200-m-thick ice. Due to the fragmentation of magma, heat flux from the magma to the surrounding ice and water was high, $\sim 1\text{--}4 \text{ MW m}^{-2}$ (Magnússon et al., 2012). Meltwater was therefore generated rapidly within the first hours of the eruption and conditions allowed meltwater to accumulate before it was released in high discharge jökulhlaups. Conditions were different when lava started to advance under the ice. The lower heat flux caused slower meltwater generation, and discharge occurred over a much longer period of time. Therefore, the hazard from the jökulhlaups was much lower during the effusive phase than the first explosive phase. Risk associated with the advancing lava relates to temporary ponding of meltwater, and it is released in small, pulsating flash floods. The threat posed can therefore be more localized, possibly mostly confined to the vicinity of the glacier terminus.

Conclusions

The total volume of lava erupted during the 2010 Eyjafjallajökull eruption is $2.5 \pm 0.6 \cdot 10^7$, and it covers an area of $0.55 \pm 0.10 \text{ km}^2$. The 2010 lava flow is divided into two types: a subglacial lava flow which was emplaced first and under the glacier. It interacted extensively with meltwater. The subaerial lava flow was emplaced after an ice canyon had been formed and flowed subaerially with limited meltwater interaction. The subglacially emplaced lava flow is larger and accounts for about 90 % of the total lava output.

Continuous meltwater generation from ice melting has an important influence on the advance of the subglacial lava flow due to the formation of ice tunnels and the thermal extraction from the lava. Meltwater expanded tunnels in front of the lava flow as it advanced, allowing the lava to move further and more rapidly beneath the ice. The rapid downslope movement of meltwater and lava was also controlled by the slope of the bedrock and the pre-eruption ice thickness.

Thermal constraints based on field observations and measurements indicate that about 45 % of the total heat of the subglacially emplaced lava was used for ice melting, about 4 % was advected away from the glacier as warm water and about 1 % was released as steam to the atmosphere. The remaining 50 % was stored in the lava, mostly in the 80–100-m-thick pile in the caldera to the north of the craters.

The heat was mostly released by forced convection of fast-flowing meltwater with heat fluxes of $125\text{--}310 \text{ kWm}^{-2}$.

Our emplacement model for the lava accounts for the complex lava-ice interactions that occurred when lava flowed inside subglacial tunnels down the Gigjökull outlet glacier for 3.2 km.

Acknowledgments We thank the Icelandic Coast Guard for their highly professional work during the eruption in Eyjafjallajökull 2010. Funding for observation flight was provided through the emergency response of the Icelandic Government. Part of the work for processing was funded by the University of Iceland Research Fund. Þórdís Högnadóttir was in charge of the observation flight programme and John Stevenson provided helpful discussion after being in the field. We thank J. Ciarrocca, R. Rossi, J. Haklar and E. Was for assistance with fieldwork at Gigjökull, which was funded in part by the U.S. National Science Foundation (RAPID EAR 1039461 to BE) and the National Geographic Committee for Research and Exploration (Grant Number 9152-12 to BE). Katharine Cashman, Dave Mcgarvie and anonymous reviewer provided helpful comments that improved the manuscript.

References

- Arason P, Petersen GN, Björnsson H (2011) Observations of the altitude of the volcanic plume during the eruption of Eyjafjallajökull, April–May 2010. *Earth System Science Data* 3(1):9–17
- Belousov A, Behncke B, Belousov M (2011) Generation of pyroclastic flows by explosive interaction of lava flows with ice/water-saturated substrate. *J Volcanol Geotherm Res* 202:60–72
- Cengel YA, Boles MA (2006) *Thermodynamics: an engineering approach*. McGraw-Hill Higher Education, Boston
- Delgado-Granados H, Miranda PJ, Núñez GC, Alzate BP, Mothes P, Roa HM, Cáceres-Correa BE, Ramos JC (2015) Hazards at ice-clad volcanoes: phenomena, processes, and examples from Mexico, Colombia, Ecuador, and Chile. In: Haerberli W, Whiteman C (eds) *Snow and ice-related hazards, risks and disasters*. Elsevier, Amsterdam, pp. 607–646
- Edwards BR, Magnússon E, Thordarson T, Gudmundsson MT, Höskuldsson Á, Oddsson B, Haklar J (2012) Interactions between lava and snow/ice during the 2010 Fimmvörðuháls eruption, south-central Iceland. *J Geophys Res* 117:B04302. doi:10.1029/2011JB008985
- Edwards BR, Gudmundsson MT, Russell JK (2015a) Glaciovolcanism. In: Sigurdsson H, Houghton B, Rymer H, Stix J, McNutt S (eds) *The encyclopedia of volcanoes*. Academic, San Diego ISBN: 9780123859389, pp. 377–393
- Edwards BR, Belousov A, Belousova M, Melnikov D (2015b) Observations on lava, snowpack and their interactions during the 2012–13 Tolbachik eruption, Klyuchevskoy Group, Kamchatka. *J Volcanol Geotherm Res*. doi:10.1016/j.jvolgeores.2015.04.009
- Gudmundsson MT, Sigmundsson F, Björnsson H (1997) Ice-volcano interaction of the 1996 Gjalp subglacial eruption, Vatnajökull, Iceland. *Nature* 389:954–957
- Gudmundsson MT (2003) Melting of ice by magma–ice–water interactions during subglacial eruptions as an indicator of heat transfer in subaqueous eruptions. In: White JDL, Smellie JL, Clague D (eds) *Geophys. Monogr.* 140. Explosive subaqueous volcanism, AGU, pp. 61–72
- Gudmundsson MT, Sigmundsson F, Björnsson H, Högnadóttir T (2004) The 1996 eruption at Gjalp, Vatnajökull ice cap, Iceland: course of events, efficiency of heat transfer, ice deformation and subglacial water pressure. *Bull Volcanol* 66:46–65
- Gudmundsson MT (2005) Subglacial volcanic activity in Iceland. In: Caseldine CJ, Russell A, Hardardóttir J, Knudsen Ó (eds) *Iceland: modern processes, past environment*. Elsevier, Amsterdam, pp. 127–151
- Gudmundsson MT, Larsen G, Höskuldsson Á, Gylfason ÁG (2008) Volcanic hazards in Iceland. *Jökull* 58:251–268
- Gudmundsson MT, Thordarson T, Höskuldsson Á, Larsen G, Björnsson H, Prata AJ, Oddsson B, Magnússon E, Högnadóttir T, Pedersen GN, Hayward CL, Stevenson JA, Jónsdóttir I (2012) Ash generation and distribution from the April–May 2010 eruption of Eyjafjallajökull, Iceland. *Sci Reports* 2:572
- Griffiths RW (2000) The dynamics of lava flows. *Annu Rev Fluid Mech* 32:477–518
- Höskuldsson A, Sparks RSJ (1997) Thermodynamics and fluid dynamics of effusive sub-glacial eruptions. *Bull Volcanol* 59(3):219–230
- Höskuldsson Á, Sparks RSJ, Carroll MR (2006) Constraints on the dynamics of subglacial basalt eruptions from geological and geochemical observations at Kverkfjöll, NE-Iceland. *Bull Volcanol* 68:689–701
- Jakobsson SP, Gudmundsson MT (2008) Subglacial and intraglacial volcanic formations in Iceland. *Jökull* 58:179–197
- Jóhannesson T et al. (2011) LiDAR mapping of the Snæfellsjökull ice cap, western Iceland. *Jökull* 61:19–32
- Jóhannesson T, Björnsson H, Magnússon E, Guðmundsson S, Pálsson F, Sigurðsson O, Thorsteinsson T, Berthier E (2013) Ice-volume changes, bias estimation of mass balance measurements and changes in subglacial lakes derived by lidar mapping of the surface Icelandic glaciers. *Ann Glaciol* 54:63–74. doi:10.3189/2013AoG63A422
- Keiding J, Sigmarsson O (2012) Geothermobarometry of the 2010 Eyjafjallajökull eruption: new constraints on Icelandic magma plumbing systems. *J Geophys Res* 117:BC00C09. doi:10.1029/2011JB008829
- Keszthelyi L, Self S, Thordarson T (2006) Flood basalts on earth, Io and Mars. *J Geol Soc* 163:253–264
- Larsen G, Dugmore AJ, Newton AJ (1999) Geochemistry of historical age silicic tephra in Iceland. *The Holocene* 9(4):463–471
- Larsen G (2002) A brief overview of eruptions from ice-covered and ice-capped volcanic systems in Iceland during the past 11 centuries: frequency, periodicity and implications. In: Smellie JL, Chapman MG (eds) *Volcano-ice interactions on earth and mars*, vol 202. Geological society, London Special Publication, pp. 81–90
- Lescinsky DT, Fink JH (2000) Lava and ice interaction at stratovolcanoes: use of characteristic features to determine past glacial extents and future volcanic hazards. *J Geophys Res* 105(B10):23,711–23,726
- Major JJ, Newhall GC (1989) Snow and ice perturbation during historical volcanic eruptions and the formation of lahars and floods. *Bull Volcanol* 52:1–27
- Magnússon E, Gudmundsson MT, Sigurdsson G, Roberts MJ, Höskuldsson F, Oddsson B (2012) Ice-volcano interactions during the 2010 Eyjafjallajökull eruption, as revealed by airborne radar. *J Geophys Res* 117:B07405
- Marzano FS, Lamantea M, Montopoli M, Di Fabio S, Picciotti F (2011) The Eyjafjallajökull explosive volcanic eruption from a microwave weather radar perspective. *Atmos Chem Phys* 11:9503–9518
- McGarvie DW (2009) Rhyolitic volcano–ice interactions in Iceland. *J Volcanol Geotherm Res* 185(4):367–389
- Moore JG (1975) Mechanism of formation of pillow lava. *Am Sci* 63: 269–277
- Moreno H, Fuentealba G (1994) The May 17–19 1994 Llaima volcano eruption, southern Andes (38° 42′ S–71° 44′ W). *Rev Geol Chile* 21: 167–171
- Morton BR, Taylor GI, Turner JS (1956) Turbulent gravitational convection from maintained and instantaneous sources. *Proc Roy Soc London A234*:1–23
- Naranjo JA, Moreno H, Banks NG (1993) La erupción del volcán Hudson en 1991 (467S), Región XI, Aisén, Chile. *Serv Nac Geol Min Bol* 44:1–50

- Naranjo JA, Moreno H (2004) Pucón town laharic debris-flow hazards from Villarrica volcano, Southern Andes (39,4°S): causes for different scenarios. In: Lara L, Clavero J (eds) Villarrica volcano. Servicio Nacional de Geología y Minería, Boletín N° 61, Southern Andes pp 72
- Oddsson B, Gudmundsson MT, Sonder I, Zimanowski B, Schmid A (2016) Experimental studies of heat transfer at the dynamic magma ice/water interface, application to subglacially emplaced lava. *J Geophys Res Solid Earth*. doi:10.1002/2016JB012865
- Óskarsson BV (2009) The Skerin ridge on Eyjafjallajökull, south Iceland: morphology and magma-ice interaction in an ice-confined silicic fissure eruption. Master thesis, University of Iceland, Reykjavík
- Paterson WSB (1994) *The Physics of Glaciers* (Third Edition), Pergamon, Amsterdam, P 378–409
- Pedersen R, Sigmundsson F (2006) Temporal development of the 1999 intrusive episode in the Eyjafjallajökull volcano, Iceland, derived from InSAR images. *Bull Volcanol* 68:377–393
- Pierson TC, Janda RJ, Thouret JC, Borrero CA (1990) Perturbation and melting of snow and ice by the 13 November 1985 eruption of Nevado-del Ruiz, Columbia, and consequent mobilization, flow and deposition of lahars. *J Volcanol Geotherm Res* 41:17–66
- Pollock M, Edwards BR, Hauksdottir S, Alcom R, Bowman L (2014) Geochemical and lithostratigraphic constraints on the formation of pillow-dominated Tindars from Undirhlíðar Quarry, Reykjanes Peninsula, Southwest Iceland. *Lithos* 200–201:317–333. doi:10.1016/j.lithos.2014.04.023
- Sigmundsson F, Hreinsdóttir S, Hooper A, Árnadóttir T, Pedersen R, Roberts MJ, et al. (2010) Intrusion triggering of the 2010 Eyjafjallajökull explosive eruption. *Nature* 468:426–430. doi:10.1038/nature09558
- Schopka HH, Gudmundsson MT, Tuffen H (2006) The formation of Helgafell, southwest Iceland, a monogenetic subglacial hyaloclastite ridge: sedimentology, hydrology and volcano—ice interaction. *J Volcanol Geotherm Res* 152:359–377
- Stevenson JA, McGarvie DW, Smellie J, JS G (2006) Subglacial and ice-contact volcanism at the Öraefajökull stratovolcano, Iceland. *Bull Volcanol* 68(2006):737–752
- Stevenson JA, Gilbert JS, McGarvie DW, Smellie JL (2011) Explosive rhyolite tuya formation: classic examples from Kerlingarfjöll, Iceland. *Quat Sci Rev* 30:192–209. doi:10.1016/j.quascirev.2010.10.011
- Strachan S (2001) A geophysical investigation of the Eyjafjallajökull glaciovolcanic system, South Iceland, using radio echo sounding. University of Edinburgh, PhD thesis, 200 pp
- Sturkell E, Sigmundsson F (2003) Recent unrest and magma movements at Eyjafjallajökull and Katla volcanoes, Iceland. *J Geophys Res* 108: 1–12
- Tuffen H, Pinkerton H, McGarvie DW, Gilbert JS (2002) Melting of the glacier base during a small-volume subglacial rhyolite eruption: evidence from Bláhnúkur, Iceland. *Sediment Geol* 149:183–198
- Tuffen H, McGarvie DW, Pinkerton H, Gilbert J, Brooker RA (2008) An explosive-intrusive subglacial rhyolite eruption at Dalakvisl, Torfajökull, Iceland. *Bull Volcanol* 70(7):841–860 **20 p**
- Tuffen H (2010) How will melting of ice affect volcanic hazards in the twenty-first century? *Philosophical transactions of the royal society A* 368(1919): 2535–2558
- Waythomas CF (2014) Water, ice and mud: lahars and lahar hazards at ice- and snow-clad volcanoes. *Geol Today* 30(1):34–39
- Wilson L, Head JW (2002) Heat transfer and melting in subglacial basaltic volcanic eruptions: implications for volcanic deposit morphology and meltwater volumes. In: Smellie JL, Chaapman, MG (eds) *Volcano-ice interactions on earth and mars*. *Geol Soc Lond, Spec Publ* 202:5–26
- Wilson L, Head JW (2007) Heat transfer in volcano-ice interactions on Earth. *Ann Glaciol* 45:83–86. doi:10.3189/172756407782282507
- Witham CS (2005) Volcanic disasters and incidents: a new database. *J Volcanol Geotherm Res* 148:191–233
- Wooster MJ, Wright R, Blake S, et al. (1997) Cooling mechanisms and an approximate thermal budget for the 1991–1993 Mount Etna lava flow. *Geophys Res Lett* 24(24):3277–3280